Rapid and Reproducible Characterization of the Wavelength Dependence of Aquatic Photochemical Reactions Using Light Emitting Diodes (LEDs)

Authors: Collin P. Ward[1*], Jennifer C. Bowen[2], Danielle H. Freeman[1,3], and Charles M. Sharpless[4]

Affiliations:

[1]Department of Marine Chemistry and Geochemistry, Woods Hole Oceanographic Institution, Woods Hole, Massachusetts 02543, USA.

[2]Department of Earth and Environmental Sciences, University of Michigan, Ann Arbor, MI, 48109, USA.

[3] MIT-WHOI Joint Program in Oceanography/Applied Ocean Science & Engineering, Cambridge and Woods Hole, MA, USA

[4]Andlinger Center for Energy and the Environment, Princeton University, Princeton, NJ, 08540, USA

Corresponding author: Collin Ward, cward@whoi.edu

TOC Graphic:

ABSTRACT

Arguably the largest knowledge gap in the aquatic photochemistry discipline is the wavelength dependence of sunlight-driven reaction rates in surface waters. Here, we introduce a new light-emitting diode (LED) based approach to directly quantify the wavelength dependence of aquatic photochemical reaction rates. The LEDs generate narrow-banded, spatially uniform light at five wavelengths (275, 309, 348, 369, and 406 nm), with irradiances that are very stable and easily adjusted to desired levels. Strong agreement was observed between irradiance measurements in each LED reactor using chemical actinometry and spectroradiometry. Apparent quantum yield (AQY) spectra of photochemical oxygen consumption by Suwannee river organic matter were determined four times across a six-month period. The shape and magnitude of the AQY spectra were highly reproducible, as indicated by strong exponential fits ($R^2 \geq 0.98$) and low variability in oxidation rates across the four trials (coefficient of variation = ~10%). This LED-based approach is cost-effective, high-throughput, and portable, allowing a broader community to study the wavelength dependence of aquatic photochemical processes in more detail than was previously possible. We anticipate that this approach will substantially advance our understanding of the wavelength dependence of photochemical reactions in surface waters and improve the accuracy of kinetic models.

INTRODUCTION

Aquatic photochemistry is an interdisciplinary field that examines how sunlight-driven reactions impact the fate and composition of diverse materials in surface waters, including major and minor elements (e.g., C,[1-14] N,[15,16] O,[17,18] S,[19] P,[20] Fe,[21,22] & Mn[23]), inorganic and organic pollutants (e.g., heavy metals,[24,25] crude oil,[26–28] pharmaceuticals and personal care products,[29,30] pesticides,[31] & plastics[32,33]), and biomolecules (e.g., lipids,[34,35] amino acids,[36,37] and pigments[38]). Accurate assessment of photochemical processes requires information about the reaction kinetics, which depend on the light available at different wavelengths throughout the water column and the photochemical reaction efficiency, or apparent quantum yield (AQY; mol product per mol light absorbed) at those wavelengths.

For simplicity, most aquatic photochemistry studies are conducted under broadband light (natural or simulated) to estimate reaction rates in sunlight, but this approach does not provide information about the AQY wavelength dependence (AQY spectra). Approaches for examining wavelength dependence have historically had several drawbacks, including low sample throughput, that have made work in the area difficult. Consequently, there is a large knowledge gap around AQY spectra, particularly for complex photosensitizers, such as dissolved and particulate organic matter.[4,5,7,12,39–41] This limits our ability to model many photochemical reactions in surface waters and, in turn, incorporate sunlight-driven processes into Earth system models.

To measure AQY spectra, two traditional approaches exist: monochromatic and polychromatic. The monochromatic approach either uses high powered lasers[42] or combines a high-power broadband light source (e.g., Xe or Hg arc) with a discrete band wavelength selection device (e.g.,

monochromator or band pass filters) to approximate monochromatic light.[15,17,43] Major benefits of this approach are that AQYs are measured directly and that photon dose-dependence,[7,17,43] or the change in reaction rate over time due to increased light absorption, can be controlled for. Major limitations of this approach are sample-throughput, cost, and portability and, in the case of laser excitation, the potential for environmentally irrelevant multiphoton phenomena. In contrast, the polychromatic approach improves throughput and can modestly reduce equipment cost.[43,44] In this approach, a series of long pass optical filters is used to progressively cut off shorter wavelength portions of an arc source spectrum, and the difference in reaction rates and light absorption rates obtained between successive filters is used to calculate AQYs. The major benefit of this approach is high sample throughput because numerous vials are simultaneously exposed to different wavelengths. A major limitation is that the shape of the AQY spectrum is typically assumed (e.g., exponential or linear decay with wavelength), which can produce inaccurate AQY spectra. Another limitation is the inability to easily control for photon dose-dependence of the kinetics occurring under each filter.[45] Further, because this approach involves determining the reaction and light absorption rate differences between pairs of filters to calculate AQYs, it inherently generates larger errors than the monochromatic approach. Finally, because the polychromatic approach, like the monochromatic approach, uses high power light sources and optical filters, it, too, is relatively expensive and not easily portable.

Advances in light-emitting diode (LED) technology over the past decade may provide a means to overcome the many limitations of the monochromatic and polychromatic approaches to measure AQYs of aquatic photochemical processes. The advantages of LEDs are numerous, including relatively low costs, small size, high efficiency, long operating lifetimes, emission of spatially

uniform, narrow-banded light, and easy control over irradiance via the power supply current.[46] This technology has already revolutionized the indoor/outdoor lighting and agricultural industries, and it is being readily adopted by the water and wastewater disinfection research community.[46] While the call to replace arc lamps with LEDs has been made[47], the aquatic photochemistry community has yet to adopt an LED-based approach to spectrally resolve the wavelength dependence of photochemical reactions in surface waters.

Here, we describe a new LED-based instrument capable of directly assessing the wavelength dependence of aquatic photochemical reactions and overcoming many disadvantages of existing approaches (e.g., cost, sample-throughput, portability), while generating data of high reproducibility and quality. We anticipate that this approach will permit rapid growth in knowledge about the wavelength dependence of a wide variety of photochemical reactions in surface waters and, consequently, improve the accuracy of photochemical kinetic models.

MATERIALS AND METHODS

Description of the LED Reactor Assembly

Each LED reactor is comprised of an inner housing, containing the samples, and an outer housing, on which is affixed an LED chip (Figure 1; Appendix S1). On top of the outer housing is a washer that provides the base for the LED chips, which are mounted to a printed circuit board and a heat sink. Passive cooling by the heat sink is sufficient to maintain the samples at room temperature, 22 ± 1 °C, without any additional cooling. The LED chips face down toward the inner housing which contains four quartz tubes. The inner housing is machined specifically for the dimensions of the tubes but can accommodate a variety of reaction vessel shapes and sizes depending on the

reaction of interest. Both housings are painted black matte to minimize light scattering and to decrease stray light in the laboratory. A separate power supply is used for each reactor. A detailed protocol for reactor assembly, validation, and use is provided in Appendix S1.

Spectroradiometry and Chemical Actinometry

Spectral irradiance measurements in all reactors were made with a NIST-calibrated Black Comet spectroradiometer equipped with a cosine corrector (StellarNet Inc.; Appendix S1). Chemical actinometry was assessed in the 309, 348, 369, and 406 nm reactors by measuring the hydroxylation of benzoic acid to salicylic acid in the presence of nitrite.[48] Actinometry was not assessed in the 275 nm reactor because the AQY of salicylic acid production has not been reported at that wavelength.[48] Salicylic acid production was quantified fluorometrically using an Aqualog (Horiba Scientific).

Photochemical Oxidation Experiments

Photochemical oxidation (dissolved O_2 consumption) experiments were conducted as an example test of the LED reactors' long-term precision in measuring AQY spectra and oxidation rates. These experiments used Suwannee River natural organic matter (SROM; 2R101N) acquired from the International Humic Substances Society (http://humic-substances.org/). In total, six experiments were conducted over a six-month period using four replicate solutions of SROM. Triplicate experiments were conducted for one SROM solution on three consecutive days (referred to as experiments 2a, 2b, and 2c). The coefficient of variation (CV) of photochemical oxidation rates was 11%. To simplify the presentation, the averaged results of experiments 2a, 2b, and 2c are

137 presented in the main text as experiment 2. All results from the oxidation experiments are
138 summarized in Table S2. The 406 nm LED reactor was only included for experiments 3 and 4.
139
140 Before each experiment, solutions of SROM were prepared in Milli-Q water (Millipore) at a
141 concentration of 20 mg SROM L^{-1} (~10 mg C L^{-1}). The solutions were adjusted to pH 7.0 ± 0.1
142 and allowed to equilibrate on a stir-plate for 24 hours prior to filtration with a 0.2 µm Sterivex
143 filter (Millipore). SROM was then transferred to Milli-Q rinsed quartz tubes (15 mm outer
144 diameter, 100 mm length; Technical Glass Products, Inc.) and sealed with a Viton-lined GL-18
145 cap with no headspace. The tubes were placed vertically in the inner housing with the flat bottom
146 facing the LED. To minimize the impact of photon dose-dependence (i.e., the change in AQY as
147 the samples absorb more light over time),[5,39,47] we adjusted the emission intensity of the LEDs via
148 the power supplies such that the moles of photons absorbed by SROM under all LEDs were equal
149 within 5% (Figure 2b; Table S2). The total number of moles of photons absorbed by SROM was
150 calculated by multiplying rates of light absorption (Q_a; mol photons m^{-2} s^{-1}, determined via
151 equation 1) by the exposed surface area of the quartz tubes (1.1 cm^2) and the time of the light
152 exposure (43,200 s).

153 $$Q_a = \sum_{\lambda_{min}}^{\lambda_{max}} E_{0_\lambda}(1 - e^{-a_{SROM_\lambda} * z}) \quad (1)$$

154 Here, E_{0_λ} is the incident photon spectral irradiance reaching the quartz tube (mol photon m^{-2} s^{-1}
155 nm^{-1}) determined with 1-nm resolution and the summation is performed with 1-nm increments
156 across the relevant wavelengths for each LED (e.g., 332 to 376 nm for the 348 nm LED). Naperian
157 absorption coefficients of SROM (a_{SROM_λ}; m^{-1}) were measured using a Perkin Elmer 650
158 spectrophotometer and calculated as the geometric mean of the light-exposed and dark control
159 treatments to account for photo-bleaching, which was minimal in all experiments (< 5%). The

pathlength (z) was 10 cm, equivalent to the height of each vial. Photochemical O_2 consumption was calculated as the concentration of dissolved O_2 in the dark-control tubes minus that in the light-exposed tubes using membrane inlet mass spectrometry (Bay Instruments, Inc.).[1,13,26,49] At all wavelengths tested, O_2 concentrations decreased linearly with exposure time (Figure S1).

Apparent Quantum Yields and Water Column Rate Modelling

Apparent quantum yields (AQYs) for the photochemical oxidation of SROM (Φ_{PO_λ}; mol O_2 mol photons^{-1}) were calculated for each tube in each LED reactor by dividing the moles of O_2 consumed by SROM by the moles of photons absorbed by SROM. For purposes of modelling exercises, the AQY data were fit to an exponential curve with 1-nm increments.

Water column rates of SROM photochemical oxidation were calculated via:

$$\text{Photochemical Oxidation (mol } O_2 \text{ m}^{-2} \text{ d}^{-1}) = \sum_{280\ nm}^{400\ nm} Q_{a_\lambda} \Phi_{PO_\lambda} \quad (2)$$

where Q_{a_λ} was calculated at each wavelength via equation (1) assuming constant: (i) incident spectral irradiance (E_{0_λ}) equal to that of clear-sky noon sunlight at 30°N,[46] (ii) a_{SROM_λ} of the SROM solutions used in the experiments, and (iii) water depth of 2 m. Summation of rates was performed with 1-nm increments from 280 to 400 nm. The goal of this modelling exercise was not to calculate actual rates of OM photochemical oxidation in the Suwannee River, but rather to determine the sensitivity of calculated water column rates to variability in the AQY spectra.

RESULTS AND DISCUSSION

Characterization of Irradiance in the LED Reactors

To confirm that the light measured by radiometry was representative of the light inside the quartz tubes, we compared the radiometric irradiance at 309, 348, 369, and 406 nm to that obtained by nitrite actinometry (Table S1). The difference between radiometry and actinometry irradiance measurements ranged from 5 to 18%, with an average of 10%. A comparison at 348 nm was made three times over a six-month period to test the reactor performance over time. In these trials, the difference between radiometry and actinometry irradiance measurements ranged from 5 to 12% (Table S1). The strong agreement between radiometry and chemical actinometry (Table S1) validates the reactor's ability to correctly determine AQYs (i.e., radiometry correctly predicts the actinometer AQY).

Radiometry was then used to further evaluate the irradiance in each LED reactor. Spatial variability of irradiance across the four vial positions was low in each reactor (<10%; Table S1). The irradiance bands were reasonably sharp; full width at half maximum (FWHM) of the bands ranged from 9 to 17 nm (Figure 2a). Irradiance increased linearly with increasing LED current across the range recommended by the manufacturer ($R^2 \geq 0.99$, Figure S2). The peak wavelength and the FWHM of the peaks were stable (± 1 nm) across all current settings. Irradiance for a given LED was independent of power supply, varying by only 1% across the five supplies used in the reactor assembly (Figure S3). Lastly, when using the reactor assembly outdoors, light contamination from natural sunlight was <1% (Figure S4).

Assessment of DOC Photochemical Oxidation Using the LED Reactor Assembly

Photochemical oxidation of SROM led to AQY spectra for all four experiments that were similar in shape and magnitude, indicating high precision of the reactor assembly over an extended time

period (Figure 2c). AQY values decreased approximately exponentially with increasing wavelength ($R^2 \geq 0.98$). The fits to a linear decay model were comparatively worse ($R^2 \geq 0.89$). The average CV of AQY values ranged from 8 to 14% at 309 and 406 nm, respectively (Table S2). The variability was largely driven by the manual radiometry measurements (CV = 5 to 10%; Table S1) rather than light absorption and O_2 consumption measurements (CV < 1%). Future automation or mechanical sensor control of the radiometry measurements may reduce the uncertainty of AQY values determined using the LED reactors.

The AQY values reported in this study are comparable to those previously reported for other terrestrial OM sources.[17] For example, at 309 nm, we report an AQY of 1.3 ± 0.1 mmol O_2 mol photons^{-1}, similar to AQYs at 310 nm reported for Shark River OM of 1.8 ± 0.1 mmol O_2 mol photons^{-1}.[17] Although the magnitudes of AQYs were similar, the shapes of the AQY spectra between studies were different. AQYs determined using the LED reactor decayed exponentially with wavelength, whereas Andrews *et al.*[17] reported that their data were best fit linearly with wavelength. This discrepancy could be explained by natural variabilities in the shape of AQY spectra between DOC sources, unequal photon doses for the modelled AQY values in Andrews *et al.*[17], or, as previously discussed,[50] no correction for inner-filter effects.

To examine how the variability in AQY spectra translates into variability of modelled SROM photochemical oxidation rates, we calculated rates throughout a 2 m deep water column under clear-sky summer conditions at 30°N (Figure 2d). For all experiments, the action spectra peaked at 330 nm. The average rate of SROM photochemical oxidation was 2.5 ± 0.3 mmol O_2 m^{-2} d^{-1}. Given the previously established high precision (long-term reproducibility) and accuracy

(radiometry agreement with actinometry), we believe this new reactor design is well-suited to test the long-standing hypothesis that photochemical oxidation of DOC may influence the dissolved O_2 cycle in surface waters[1,17] and, thus, the accuracy of O_2 based methods used to infer the metabolic state of aquatic ecosystems.[50]

Five Key Advantages of LEDs for Wavelength Dependence Studies

This study describes an LED-based reactor assembly capable of quantifying the wavelength dependence of aquatic photochemical reactions. There are five key benefits of this new approach. First, the narrow bandwidth (FWHM = ~15 nm) output of LEDs provides reliable wavelength control to directly assess the spectral dependence of photochemical reactions. Available wavebands range from the deep UVC (i.e., < 280 nm, applicable to conditions on early Earth, the upper atmosphere, or UVC water treatment) to the visible (i.e., > 400 nm), allowing the user to customize reactor assemblies, including the inner housings, depending on the reactions of interest.

Second, the high power and spatial uniformity of LEDs (Figure S2, Table S1) allows for high throughput, reproducible, and direct measurement of AQY spectra (Figure 2c). The precision of AQYs determined using the LED reactor assembly (CV = 10%) is comparable to that of monochromatic systems (CV = 11%).[17] Moreover, the LED reactor assembly represents a substantial improvement over monochromatic approaches that can only measure one or two samples at a time, or polychromatic approaches that indirectly calculate AQYs from differential rates, thus increasing uncertainty in the final values.

Third, the LED-based approach is more cost-effective than current methods. Because LEDs have low energy requirements, they don't require costly ballasts or power supplies. The narrow-banded light generated by the LEDs eliminates the need for wavelength selection devices (e.g., monochromator or optical filters). The efficiency of LEDs eliminates the need for costly cooling systems like air conditioners or water baths. Instead, a $5 (USD) heat sink is sufficient to stabilize samples at room temperature. Moreover, the LED chips themselves are cost-effective compared to Xe arc lamps (~$750 for a replacement lamp). Cost-effective (<$10/W) and powerful (≥10W optical power) UVA and visible LEDs are already on the market; currently, UVB and UVC LEDs are considerably more expensive ($1000/W) and have a maximum optical power of ~100 mW. Multi-chip arrays can be assembled to increase irradiance, and power levels of individual chips are expected to increase substantially due to heightened demand for energy efficient water and air disinfection.[46] This cost advantage is especially notable when considered over the system lifetime, given that the expected lifetime of LEDs is at least 10-fold longer than Xe arc lamps (>10,000 versus 1,000 hours). Not including the quartz tubes, the entire LED reactor assembly used here is comprised of off-the-shelf parts and costs less than $2,500 to build, which is approximately five to ten times less expensive than widely used, commercial Xe arc based solar simulators (not accounting for the additional cost of a monochromator or optical filters).

Fourth, our LED reactor assembly is compact (~3 ft^3), lightweight (~20 lbs.), durable, and energy efficient (<20 W), making it operational at remote research field stations or on research cruises, potentially using a car battery and an inverter. This stands in direct contrast to arc or laser systems that are large (>12 ft^3), fragile, immobile (>200 lbs.), and energy intensive (>500 W). The ability to run photochemical experiments in the field eliminates the need to stabilize and preserve samples

for subsequent analysis in the laboratory, which may improve the overall quality of the data acquired.

Fifth, the ability to adjust irradiance (Figures 2b and S2) is a key feature that allows the user to minimize the influence of photon dose-dependence when measuring AQY spectra.[7,17,43] Dose dependence of photochemical reactions has been recognized for decades, but no high-throughput method has allowed users to account for this process. Reactor assemblies of the type described here provide the community a high-throughput approach to easily characterize photon dose-dependence, which should greatly improve the ability of photochemical kinetic models to accurately predict changes in rates over time.

Adoption of this new LED-based instrument by the aquatic photochemistry community will substantially advance our knowledge of the wavelength dependence of photochemical reactions and improve the accuracy of rate estimates. Reactions of interest may include the production of reactive intermediates, the cycling of major and minor elements, and the fate of legacy and emerging contaminants. Ultimately, the information gained from this new technology can be incorporated into Earth system models to quantify sunlight-driven processes over space and time.

Supporting information: Photochemical oxidation time series tests; irradiance vs. forward current profiles; power supply tests; natural light contamination tests; chemical actinometry vs. radiometry validation tests; experimental data for Figures 2b and 2c in the main text; Appendix describing how to build, validate, and use the LED reactor assembly.

Acknowledgements: We thank Sam McNichol for assistance with the power supply tests, and Rose Cory for discussions about the reactor designs. Funding for this work was provided in part by the Department of Fisheries and Oceans Canada Multi Partner Research Initiative project #1.06 (to CPW), the Andrew W. Mellon Foundation Endowed Fund for Innovative Research (to CPW), and the National Science Foundation Graduate Research Fellowship Program (to DHF).

Figure 1: Schematic of the LED reactors and assembly.

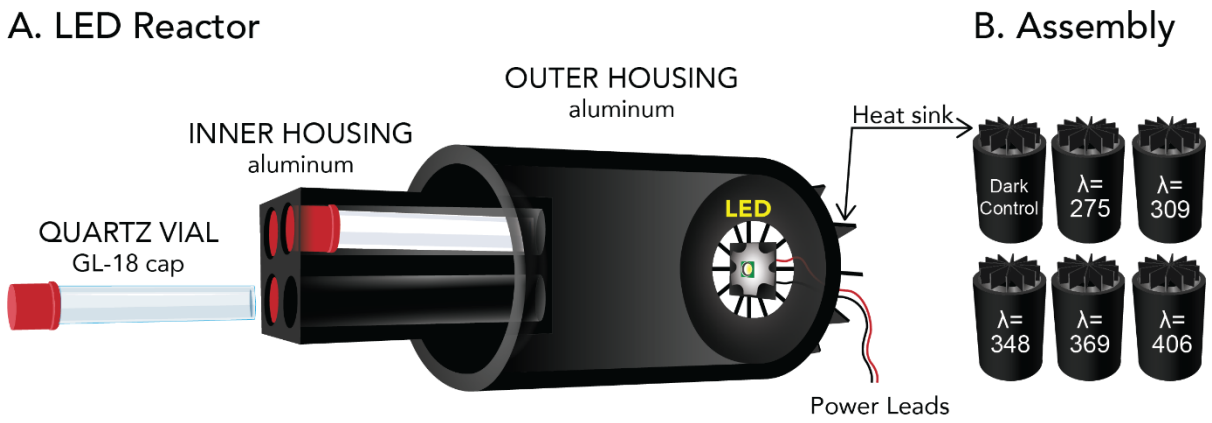

Figure 2: (A) Relative spectral photon irradiance for the five LEDs chips used in this study. The peak waveband and full width at half maximum of each peak is listed. **(B)** Moles of photons absorbed by SROM in each of the four replicate experiments. The LED emission intensity was set such that a similar amount of light was absorbed at each wavelength, which minimized the influence of photon dose-dependence on the reproducibility assessment. **(C)** Apparent quantum yield (AQY) spectra for the photochemical oxidation of SROM in each of the four replicate experiments. **(D)** Action spectra for the photochemical oxidation of SROM from 280-400 nm in each of the four replicate experiments.

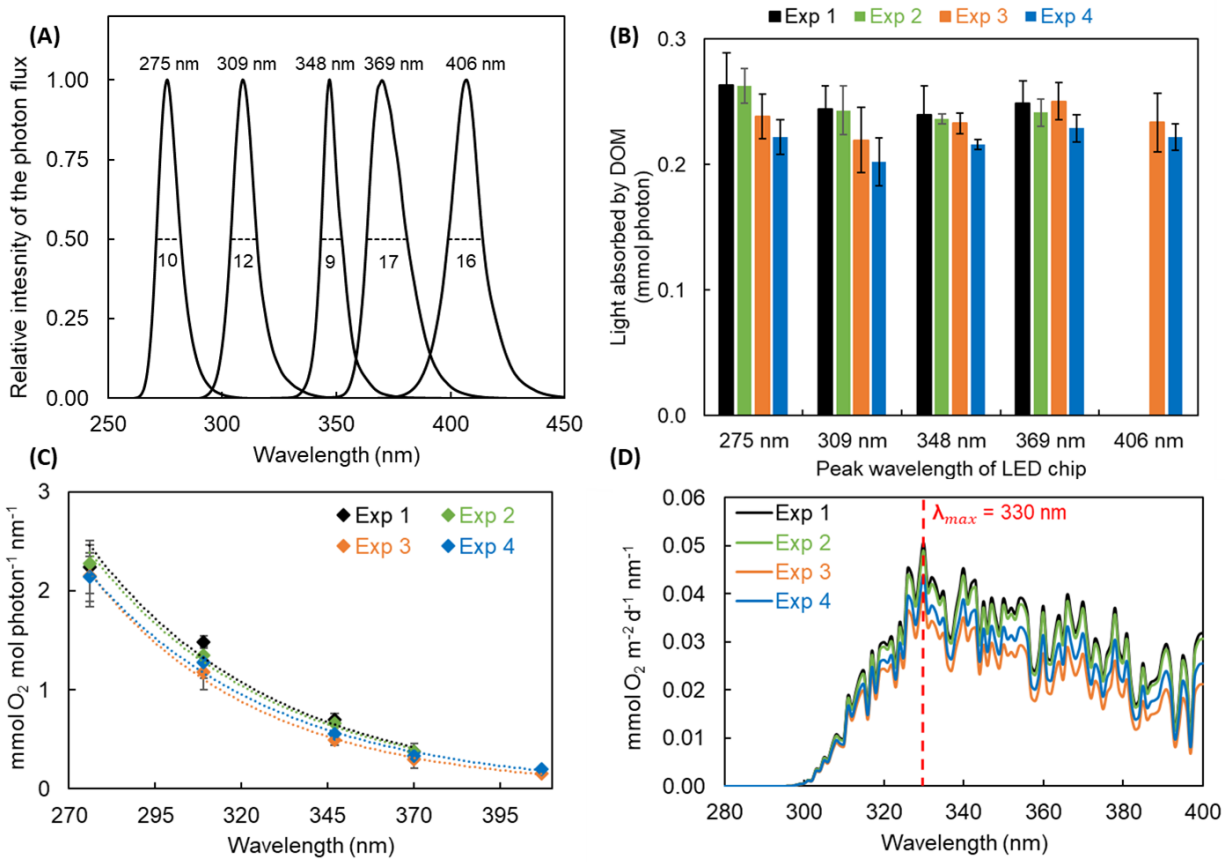

References:

(1) Cory, R. M.; Ward, C. P.; Crump, B. C.; Kling, G. W. Sunlight Controls Water Column Processing of Carbon in Arctic Fresh Waters. *Science (80-.).* **2014**, *345*, 925–928.

(2) Bowen, J. C.; Ward, C. P.; Kling, G. W.; Cory, R. M. Arctic Amplification of Global Warming Strengthened by Sunlight Oxidation of Permafrost Carbon to CO2. *Geophys. Res. Lett.* **2020**. https://doi.org/10.1029/2020GL087085.

(3) Dalrymple, R. M.; Carfagno, A. K.; Sharpless, C. M. Correlations between Dissolved Organic Matter Optical Properties and Quantum Yields of Singlet Oxygen and Hydrogen Peroxide. *Environ. Sci. Technol.* **2010**, *44* (15), 5824–5829. https://doi.org/10.1021/es101005u.

(4) Estapa, M. L.; Mayer, L. M.; Boss, E. Rate and Apparent Quantum Yield of Photodissolution of Sedimentary Organic Matter. *Limnol. Oceanogr.* **2012**, *57* (6), 1743–1756. https://doi.org/10.4319/lo.2012.57.6.1743.

(5) Kieber, D. J.; McDaniel, J.; Mopper, K. Photochemical Source of Biological Substrates in Sea Water: Implications for Carbon Cycling. *Nature* **1989**, *341* (6243), 637–639. https://doi.org/10.1038/341637a0.

(6) Latch, D. E.; McNeill, K. Microheterogeneity of Singlet Oxygen Distributions in Irradiated Humic Acid Solutions. *Science (80-.).* **2006**, *311* (5768), 1743–1747. https://doi.org/10.1126/science.1121636.

(7) Miller, W. L.; Zepp, R. G. Photochemical Production of Dissolved Inorganic Carbon from Terrestrial Organic Matter: Significance to the Oceanic Organic Carbon Cycle. *Geophys. Res. Lett.* **1995**, *22* (4), 417–420. https://doi.org/10.1029/94GL03344.

(8) Mopper, K.; Zhou, X. Hydroxyl Radical Photoproduction in the Sea and Its Potential Impact on Marine Processes. *Science (80-.).* **1990**, *250* (4981), 661–664. https://doi.org/10.1126/science.250.4981.661.

(9) Mopper, K.; Kieber, D. J.; Stubbins, A. Marine Photochemistry of Organic Matter: Processes and Impacts. In *Biogeochemistry of Marine Dissolved Organic Matter*; Hansell, D. A., Carlson, C. A., Eds.; Elsevier: New York, 2015; pp 390–431.

(10) Moran, M. A.; Zepp, R. G. Role of Photoreactions in the Formation of Biologically Labile Compounds from Dissolved Organic Matter. *Limnol. Oceanogr.* **1997**, *42* (6), 1307–1316. https://doi.org/10.4319/lo.1997.42.6.1307.

(11) Sharpless, C. M.; Aeschbacher, M.; Page, S. E.; Wenk, J.; Sander, M.; McNeill, K. Photooxidation-Induced Changes in Optical, Electrochemical, and Photochemical Properties of Humic Substances. *Environ. Sci. Technol.* **2014**, *48* (5), 2688–2696. https://doi.org/10.1021/es403925g.

(12) Song, G.; Richardson, J. D.; Werner, J. P.; Xie, H.; Kieber, D. J. Carbon Monoxide Photoproduction from Particles and Solutes in the Delaware Estuary under Contrasting Hydrological Conditions. *Environ. Sci. Technol.* **2015**, *49* (24), 14048–14056. https://doi.org/10.1021/acs.est.5b02630.

(13) Ward, C. P.; Cory, R. M. Complete and Partial Photo-Oxidation of Dissolved Organic Matter Draining Permafrost Soils. *Environ. Sci. Technol.* **2016**, *50*, 3545–3553.

(14) Zafiriou, O. Sunburnt Organic Matter: Biogeochemistry of Light-Altered Substances. *Limnol.*

Oceanogr. Bull. **2002**, *11* (4), 69–74.

(15) Gao, H.; Zepp, R. G. Factors Influencing Photoreactions of Dissolved Organic Matter in a Coastal River of the Southeastern United States. *Environ. Sci. Technol.* **1998**, *32* (19), 2940–2946. https://doi.org/10.1021/es9803660.

(16) Aarnos, H.; Ylöstalo, P.; Vähätalo, A. V. Seasonal Phototransformation of Dissolved Organic Matter to Ammonium, Dissolved Inorganic Carbon, and Labile Substrates Supporting Bacterial Biomass across the Baltic Sea. *J. Geophys. Res. Biogeosciences* **2012**. https://doi.org/10.1029/2010JG001633.

(17) Andrews, S.; Caron, S.; Zafiriou, O. Photochemical Oxygen Consumption in Marine Waters: A Major Sink for Colored Dissolved Organic Matter? *Limnol. Oceanogr.* **2000**, *45* (2), 267–277.

(18) Ward, C. P.; Sharpless, C. M.; Valentine, D. L.; Aeppli, C.; Sutherland, K. M.; Wankel, S. D.; Reddy, C. M. Oxygen Isotopes (δ18O) Trace Photochemical Hydrocarbon Oxidation at the Sea Surface. *Geophys. Res. Lett.* **2019**, *46*, 6745–6754.

(19) Ossola, R.; Tolu, J.; Clerc, B.; Erickson, P. R.; Winkel, L. H. E.; McNeill, K. Photochemical Production of Sulfate and Methanesulfonic Acid from Dissolved Organic Sulfur. *Environ. Sci. Technol.* **2019**, *53* (22), 13191–13200. https://doi.org/10.1021/acs.est.9b04721.

(20) Zhang, X.; Li, J.; Fan, W.-Y.; Sheng, G.-P. Photomineralization of Effluent Organic Phosphorus to Orthophosphate under Simulated Light Illumination. *Environ. Sci. Technol.* **2019**, *53* (9), 4997–5004. https://doi.org/10.1021/acs.est.9b00348.

(21) Zepp, R. G.; Faust, B. C.; Hoigne, J. Hydroxyl Radical Formation in Aqueous Reactions (pH 3-8) of iron(II) with Hydrogen Peroxide: The Photo-Fenton Reaction. *Environ. Sci. Technol.* **1992**, *26* (2), 313–319. https://doi.org/10.1021/es00026a011.

(22) Voelker, B. M.; Morel, F. M. M.; Sulzberger, B. Iron Redox Cycling in Surface Waters: Effects of Humic Substances and Light. *Environ. Sci. Technol.* **1997**, *31* (4), 1004–1011. https://doi.org/10.1021/es9604018.

(23) Zhang, T.; Liu, L.; Tan, W.; Suib, S. L.; Qiu, G.; Liu, F. Photochemical Formation and Transformation of Birnessite: Effects of Cations on Micromorphology and Crystal Structure. *Environ. Sci. Technol.* **2018**, *52* (12), 6864–6871. https://doi.org/10.1021/acs.est.7b06592.

(24) Seller, P.; Kelly, C. A.; Rudd, J. W. M.; MacHutchon, A. R. Photodegradation of Methylmercury in Lakes. *Nature* **1996**, *380* (6576), 694–697. https://doi.org/10.1038/380694a0.

(25) Bergquist, B. A.; Blum, J. D. Mass-Dependent and -Independent Fractionation of Hg Isotopes by Photoreduction in Aquatic Systems. *Science (80-.).* **2007**, *318* (5849), 417–420. https://doi.org/10.1126/science.1148050.

(26) Ward, C. P.; Sharpless, C. M.; Valentine, D. L.; French-McCay, D. P.; Aeppli, C.; White, H. K.; Rodgers, R. P.; Gosselin, K. M.; Nelson, R. K.; Reddy, C. M. Partial Photochemical Oxidation Was a Dominant Fate of Deepwater Horizon Surface Oil. *Environ. Sci. Technol.* **2018**, *52* (4), 1797–1805. https://doi.org/10.1021/acs.est.7b05948.

(27) Ward, C. P.; Overton, E. B. How the 2010 Deepwater Horizon Spill Reshaped Our Understanding of Crude Oil Photochemical Weathering at Sea: A Past, Present, and Future Perspective. *Environ. Sci. Process. Impacts* **2020**.

(28) Payne, J. R.; Phillips, C. R. Photochemistry of Petroleum in Water. *Environ. Sci. Technol.* **1985**, *19* (7), 569–579.

(29) Yan, S.; Song, W. Photo-Transformation of Pharmaceutically Active Compounds in the Aqueous Environment: A Review. *Environ. Sci. Process. Impacts* **2014**, *16* (4), 697–720. https://doi.org/10.1039/C3EM00502J.

(30) Boreen, A. L.; Arnold, W. A.; McNeill, K. Photodegradation of Pharmaceuticals in the Aquatic Environment: A Review. *Aquat. Sci.* **2003**, *65* (4), 320–341. https://doi.org/10.1007/s00027-003-0672-7.

(31) Remucal, C. K. The Role of Indirect Photochemical Degradation in the Environmental Fate of Pesticides: A Review. *Environ. Sci. Process. Impacts* **2014**, *16* (4), 628. https://doi.org/10.1039/c3em00549f.

(32) Gewert, B.; Plassmann, M.; Sandblom, O.; MacLeod, M. Identification of Chain Scission Products Released to Water by Plastic Exposed to Ultraviolet Light. *Environ. Sci. Technol. Lett.* **2018**, *5* (5), 272–276. https://doi.org/10.1021/acs.estlett.8b00119.

(33) Ward, C. P.; Armstrong, C. J.; Walsh, A. N.; Jackson, J. H.; Reddy, C. M. Sunlight Converts Polystyrene to Carbon Dioxide and Dissolved Organic Carbon. *Environ. Sci. Technol. Lett.* **2019**, *6* (11), 669–674. https://doi.org/10.1021/acs.estlett.9b00532.

(34) Amiraux, R.; Belt, S. T.; Vaultier, F.; Galindo, V.; Gosselin, M.; Bonin, P.; Rontani, J. F. Monitoring Photo-Oxidative and Salinity-Induced Bacterial Stress in the Canadian Arctic Using Specific Lipid Tracers. *Mar. Chem.* **2017**, *194*, 89–99. https://doi.org/10.1016/j.marchem.2017.05.006.

(35) Collins, J. R.; Fredricks, H. F.; Bowman, J. S.; Ward, C. P.; Moreno, C.; Longnecker, K.; Marchetti, A.; Hansel, C. M.; Ducklow, H. W.; Van Mooy, B. A. S. The Molecular Products and Biogeochemical Significance of Lipid Photooxidation in West Antarctic Surface Waters. *Geochim. Cosmochim. Acta* **2018**, *232*, 244–264. https://doi.org/10.1016/j.gca.2018.04.030.

(36) Boreen, A. L.; Edhlund, B. L.; Cotner, J. B.; McNeill, K. Indirect Photodegradation of Dissolved Free Amino Acids: The Contribution of Singlet Oxygen and the Differential Reactivity of DOM from Various Sources. *Environ. Sci. Technol.* **2008**, *42* (15), 5492–5498. https://doi.org/10.1021/es800185d.

(37) Lundeen, R. A.; Janssen, E. M.-L.; Chu, C.; Mcneill, K. Environmental Photochemistry of Amino Acids, Peptides and Proteins. *Chim. Int. J. Chem.* **2014**, *68* (11), 812–817. https://doi.org/10.2533/chimia.2014.812.

(38) Arakawa, N.; Aluwihare, L. I.; Simpson, A. J.; Soong, R.; Stephens, B. M.; Lane-Coplen, D. Carotenoids Are the Likely Precursor of a Significant Fraction of Marine Dissolved Organic Matter. *Sci. Adv.* **2017**, *3* (9), e1602976. https://doi.org/10.1126/sciadv.1602976.

(39) Marchisio, A.; Minella, M.; Maurino, V.; Minero, C.; Vione, D. Photogeneration of Reactive Transient Species upon Irradiation of Natural Water Samples: Formation Quantum Yields in Different Spectral Intervals, and Implications for the Photochemistry of Surface Waters. *Water Res.* **2015**, *73*, 145–156. https://doi.org/10.1016/j.watres.2015.01.016.

(40) Haag, W. R.; Hoigné, J.; Gassman, E.; Braun, A. M. Singlet Oxygen in Surface Waters - Part II: Quantum Yields of Its Production by Some Natural Humic Materials as a Function of Wavelength. *Chemosphere* **1984**, *13* (5–6), 641–650. https://doi.org/10.1016/0045-6535(84)90200-5.

(41) Sharpless, C. M. Lifetimes of Triplet Dissolved Natural Organic Matter (DOM) and the Effect of NaBH 4 Reduction on Singlet Oxygen Quantum Yields: Implications for DOM Photophysics. *Environ. Sci. Technol.* **2012**, *46* (8), 4466–4473. https://doi.org/10.1021/es300217h.

(42) Partanen, S. B.; Erickson, P. R.; Latch, D. E.; Moor, K. J.; McNeill, K. Dissolved Organic Matter Singlet Oxygen Quantum Yields: Evaluation Using Time-Resolved Singlet Oxygen Phosphorescence. *Environ. Sci. Technol.* **2020**, *54* (6), 3316–3324. https://doi.org/10.1021/acs.est.9b07246.

(43) Kieber, D. J.; Miller, G. W.; Neale, P. J.; Mopper, K. Wavelength and Temperature-Dependent Apparent Quantum Yields for Photochemical Formation of Hydrogen Peroxide in Seawater. *Environ. Sci. Process. Impacts* **2014**. https://doi.org/10.1039/c4em00036f.

(44) Johannessen, S. C.; Miller, W. L. Quantum Yield for the Photochemical Production of Dissolved Inorganic Carbon in Seawater. *Mar. Chem.* **2001**, *76* (4), 271–283. https://doi.org/10.1016/S0304-4203(01)00067-6.

(45) Reader, H. E.; Miller, W. L. The Efficiency and Spectral Photon Dose Dependence of Photochemically Induced Changes to the Bioavailability of Dissolved Organic Carbon. *Limnol. Oceanogr.* **2014**, *59* (1), 182–194. https://doi.org/10.4319/lo.2014.59.1.0182.

(46) Chen, J.; Loeb, S.; Kim, J. H. LED Revolution: Fundamentals and Prospects for UV Disinfection Applications. *Environmental Science: Water Research and Technology*. 2017, pp 188–202. https://doi.org/10.1039/c6ew00241b.

(47) Hölz, K.; Lietard, J.; Somoza, M. M. High-Power 365 Nm UV LED Mercury Arc Lamp Replacement for Photochemistry and Chemical Photolithography. *ACS Sustain. Chem. Eng.* **2017**, *5* (1), 828–834. https://doi.org/10.1021/acssuschemeng.6b02175.

(48) Jankowski, J. J.; Kieber, D. J.; Mopper, K. Nitrate and Nitrite Ultraviolet Actinometers. *Photochem. Photobiol.* **1999**, *70* (3), 319–328. https://doi.org/10.1111/j.1751-1097.1999.tb08143.x.

(49) Kana, T. M.; Darkangelo, C.; Hunt, M. D.; Oldham, J. B.; Bennett, G. E.; Cornwell, J. C. Membrane Inlet Mass Spectrometer for Rapid High-Precision Determination of N2, O2, and Ar in Environmental Water Samples. *Anal. Chem.* **1994**, *66* (23), 4166–4170. https://doi.org/10.1021/ac00095a009.

(50) Kitidis, V.; Tilstone, G. H.; Serret, P.; Smyth, T. J.; Torres, R.; Robinson, C. Oxygen Photolysis in the Mauritanian Upwelling: Implications for Net Community Production. *Limnol. Oceanogr.* **2014**, *59* (2), 299–310. https://doi.org/10.4319/lo.2014.59.2.0299.